# Hydrogen Clathrate Structures in Uranium Hydrides at High Pressures

Xiao-hui Wang, Fa-wei Zheng, Zhuo-wei Gu, Fu-li Tan, Jian-heng Zhao, Cang-li Liu, Cheng-wei Sun, Jian Liu,* and Ping Zhang*

ACCESS | Metrics & More | Article Recommendations | Supporting Information

**ABSTRACT:** Room-temperature superconductivity has always been an area of intensive research. Recent findings of clathrate metal hydrides structures have opened up the doors for achieving room-temperature superconductivity in these materials. Here, we report first-principles calculations for stable H-rich clathrate structures of uranium hydrides at high pressures. The clathrate uranium hydrides contain H cages with stoichiometries of $H_{24}$, $H_{29}$, and $H_{32}$, in which H atoms are bonded covalently to other H atoms, and U atoms occupy the centers of the cages. Especially, a $UH_{10}$ clathrate structure containing $H_{32}$ cages is predicted to have an estimated $T_c$ higher than 77 K at high pressures.
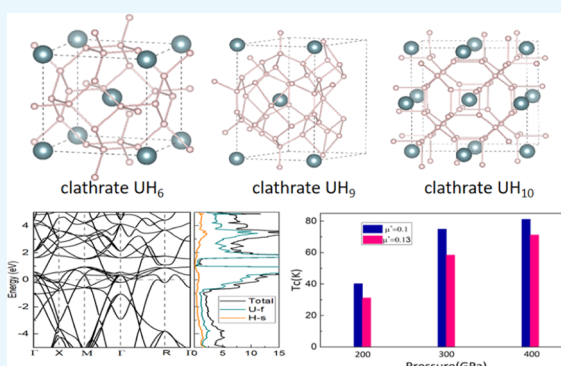
## 1. INTRODUCTION

Ever since metallic hydrogen was predicted to present high-$T_c$ phonon-mediated superconductivity,[1,2] plenty of experimental studies have been performed to realize solid metallic hydrogen[3-5] but extremely high pressure is required to get hydrogen metallization.[6] Luckily, hydrogen-rich compounds were predicted to be high-$T_c$ superconductors with significantly lowered pressures than that in pure hydrogen to attain metallic states due to the fact that hydrogen atoms in hydrogen-rich compounds have already undergone a form of "precompression".[7] Later on, numerous theoretical research studies have been implemented to search for high-$T_c$ hydrogen-rich compounds with experimentally accessible pressure, and the estimated $T_c$ of some compounds exceeds 200 K.[8-14] Especially, experimental results have reported the high-$T_c$ superconductivity of $H_3S$ and $LaH_{10}$, the $T_c$ of which are up to 183 and 260 K, respectively.[15,16] These theoretical as well as experimental results have claimed the validity of precompression effect[7] and have stimulated researchers to find more high-$T_c$ hydride superconductors.

More recently, much attention is focused on clathrate metal hydride structures. Among them, $CaH_6$,[10] $LaH_{10}$,[1313] and $YH_{10}$[14,17] were reported to have $T_c$ values above 200 K. As the research of hydrogen clathrate structures in rare earth hydrides reported, clathrate structures feature emergence of unusual H cages with stoichiometries of $H_{24}$, $H_{29}$, and $H_{32}$, with H atoms weakly covalently bonding to each other and metal atoms occupying the centers of the cages.[17,18] Various research studies on superconducting clathrate metal hydride structures are currently under investigation.[14,19,20]

In general, the high $T_c$ of metal hydrides requires that electrons of H atoms contribute mainly to the electron density of states (DOS) at the Fermi level, and one way to promote high-$T_c$ superconductivity is to search high H content metal hydrides. However, it turns out that some of these structures do not have higher $T_c$ values (such as $MgH_{16}$[21] and $AsH_8$[22]) than those which contain relatively less H ($CaH_6$[10] and $YH_6$[23]) because of the undesirable appearance of $H_2$-like molecular units in these structures, which leads to relatively lower density of states at the Fermi level.[17,20] Luckily, in these clathrate hydrides such as $LaH_{10}$[13] and $YH_{10}$,[14,17] the metal elements transfer electrons to H atoms, thus forming ionic bonds between metal elements and H atoms. Through the clathrate cages, these structures can avoid forming $H_2$-like molecular units but can still have high H contents.

In metal hydrides, many of the high $T_c$ values correspond to hydrides of metals with low-lying empty orbitals[18] (such as Th[24] and Ac[25] elements, $T_c$ of which is above 240 K). Recently, uranium hydrides were reported to have rich new compounds and many of them were expected to be high-temperature superconductors.[26] Therefore, to seek optimal solution of high-$T_c$ metal hydrides, we turn attention to clathrate-structured uranium hydrides. On the one hand,
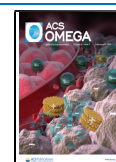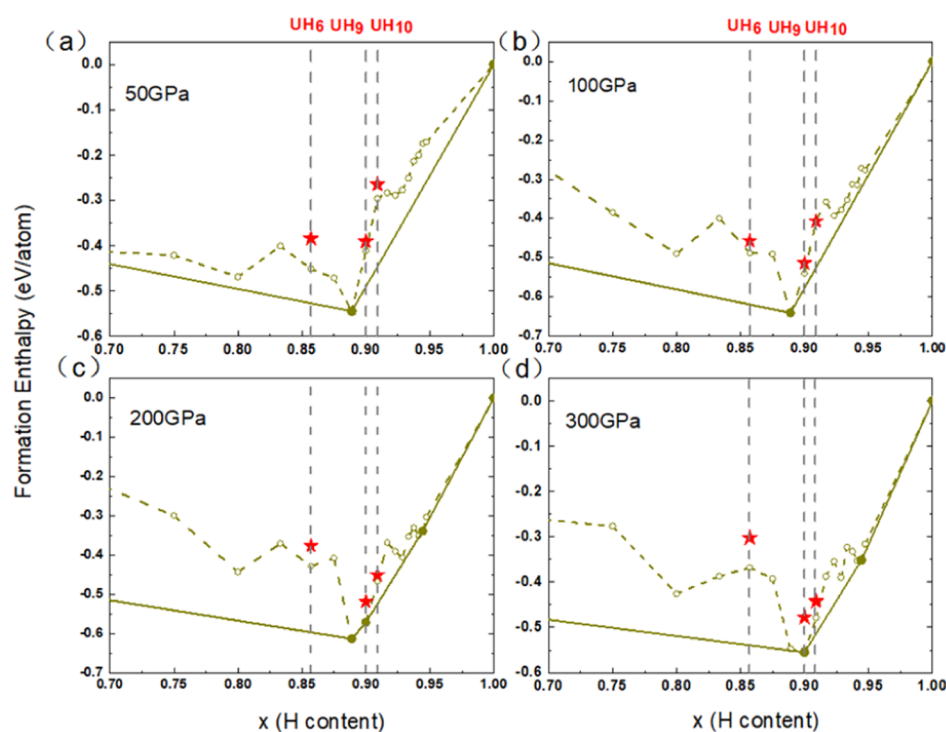
**Figure 1.** Formation enthalpies of uranium hydrides against the decomposition at high pressures. (a–d) Pressures of 50, 100, 200, and 300 GPa, respectively.
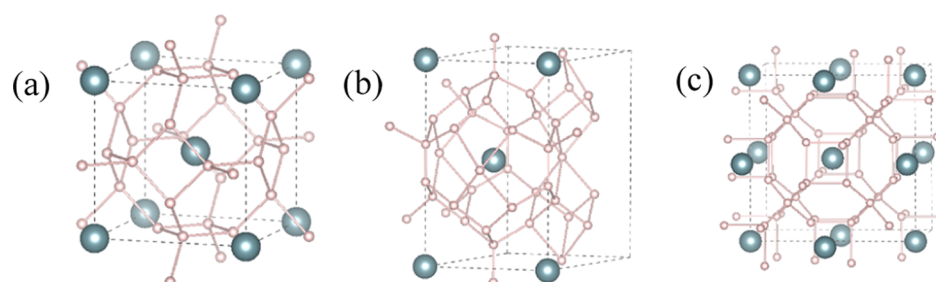


**Figure 2.** Crystal structures of clathrate $UH_x$ systems. The small and large spheres represent H and U atoms, respectively. (a–c) $Im\bar{3}m$ -$UH_6$, $P63/mmc$-$UH_9$, and $Fm\bar{3}m$-$UH_{10}$, respectively, under 300 GPa.

clathrate uranium hydride can have high H contents due to the possible high oxidation states of the uranium element. On the other hand, clathrate cages of uranium hydride can avoid $H_2$-like molecular units, increasing the thermodynamical stability of the clathrate structure. Meanwhile, the uranium element has relatively low electronegativity using the Pauling scale,[27] so uranium can easily transfer more electrons to hydrogen, thus may enhance the electron–phonon coupling (EPC) and possible superconductivity. We, here, report exploration of superconducting hydrogen clathrate structures in uranium hydrides at high pressures. The clathrate structures, electronic properties, and superconductivity are discussed below.

## 2. RESULTS AND DISCUSSION

Our previous study has reported a structure search for uranium hydrides, and the formation enthalpies of uranium hydrides against the decomposition at high pressures has been reported,[28] in which the reference phases are solid uranium and molecular hydrogen. Based on this and research on clathrate structures of rare earth hydrides,[17] the structure search for clathrate uranium hydrides was executed at high

pressures (50, 100, 200, and 300 GPa). Consequently, clathrate structures of $UH_x$ at $x$ = 6, 9, and 10 stoichiometries were found, and the convex hull diagrams against the decomposition reactions are depicted in Figure 1a–d. The energetic stabilities were obtained from their formation enthalpies relative to the decomposition. The dotted green lines show the most stable compounds under each pressure, and red five-pointed stars represent $UH_6$, $UH_9$, and $UH_{10}$ clathrate structures. To show more clearly the results of the clathrate structures, only $UH_3$–$UH_{18}$ were plotted. It can be seen that all of the formation enthalpies of the investigated $UH_6$, $UH_9$, and $UH_{10}$ clathrate structures are below zero, thus all of the compounds are stable against the decomposition. Among them, $UH_9$ and $UH_{10}$ are especially near convex hull lines, thus they are quite thermodynamically stable. The predicted $UH_9$ and $UH_{10}$ are more stable with increasing pressures as they approach the convex hull solid lines.

For the investigated $UH_6$, $UH_9$, and $UH_{10}$ clathrate structures, their space groups are $Im\bar{3}m$-$UH_6$, $P63/mmc$-$UH_9$, and $Fm\bar{3}m$-$UH_{10}$, respectively, and the crystal structures are shown in Figure 2a–c. The clathrate structures can also be seen in Figure 2, which are $H_{24}$ cages in $UH_6$, $H_{29}$ cages in
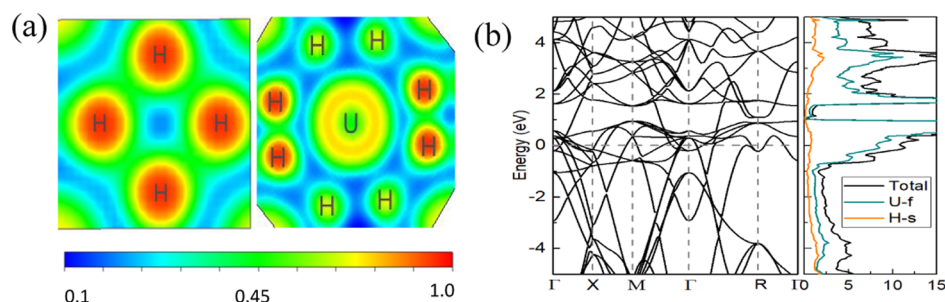
**Figure 3.** (a) ELF plots for clathrate $UH_{10}$ at 300 GPa. (b) The band structure and projected density of states (DOS) of clathrate $UH_{10}$ at 300 GPa. Projected DOS of f electrons on U and s electrons in H atoms are plotted in green and yellow lines, respectively.

$UH_9$, and $H_{32}$ cages in $UH_{10}$, respectively. These clathrate structures share the same structures with lanthanum and yttrium hydrides,[17] and clathrate $UH_9$ has the same structure with ref 26. Each $H_{24}$ cage contains six squares and eight hexagons, the $H_{29}$ cage consists of irregular squares, pentagons, and hexagons, and each $H_{32}$ cage contains 6 squares and 12 hexagons. The properties of these clathrate structures have been clearly exported, and the $UH_{10}$ clathrate structure under 300 GPa was taken as an example in the following part.

To examine the chemical bonding of the $UH_6$, $UH_9$, and $UH_{10}$ clathrate structures, the electron localization functions (ELFs)[29] were calculated, and the ELF of the $UH_{10}$ clathrate structure under 300 GPa is shown in Figure 3a. Due to the absence of charge localization between U and H atoms, it can be seen that the U–H bonding is purely ionic, while H–H interaction is weakly covalent, which can be seen from the charge localization between the nearest-neighboring H atoms. In addition, within the $H_{24}$, $H_{29}$, and $H_{32}$ cages in clathrate $UH_6$, $UH_9$, and $UH_{10}$, the nearest H–H distances are equal to 1.217, 0.98, and 1.04 Å at 300 GPa, respectively, which are much longer than that in the $H_2$ gas molecule (0.74 Å) and similar to the H–H distance (0.98 Å)[30] in monatomic solid hydrogen at 500 GPa. Then, Bader charge analysis[31,32] was executed, and it proved that electrons transfer from uranium atoms to hydrogen atoms. To be specific, about 1.3 electrons of per uranium atom transfer to the near hydrogen atoms, and every hydrogen atom can obtain 0.12–0.16 electrons. The amount of the transferred charge does not change much with the hydrogen contents and external pressure. This specific charge transferring mechanism enhances the stability of these clathrate structures.

To investigate the mechanical properties of these predicted clathrate $UH_6$, $UH_9$, and $UH_{10}$ on an atomic level, their band structures and projected DOS at high pressures were calculated and are depicted in Figures S1–S3, among which the results of the clathrate $UH_{10}$ structure under 300 GPa are depicted in Figure 3b. It can be concluded from the band structures that all of the predicted clathrate structures exhibit metallic behavior by evidence of bands crossing the Fermi level. For the same space group of clathrate $UH_6$, $UH_9$, and $UH_{10}$, the band structures and DOS look quite similar with different pressures. It can be inferred from the DOS that the major contribution of total DOS at the Fermi level is made from uranium atoms, and the DOS contribution of uranium atoms mainly consists of f electrons. Meanwhile, s electrons of H atoms contribute to the DOS around the Fermi level too. One can also see that f electrons of uranium atoms mainly lie above the Fermi level.

Phonon dispersions of these clathrate structures have been calculated, and the highest phonon vibration mode at the Γ

point for clathrate $UH_{10}$ at 300 GPa is shown in Figure 4a. The vibration mode describes the H–H bond compressing and
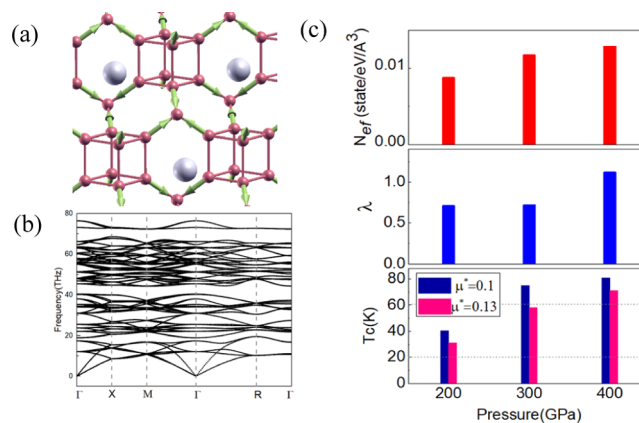


**Figure 4.** (a) Highest phonon vibration mode at the Γ point for clathrate $UH_{10}$ at 300 GPa. (b) The phonon dispersions of clathrate $UH_{10}$ at 300 GPa. (c) Electronic DOS (top panel) of H at the Fermi level ($N_{Ef}$) per Å³, the EPC parameter $\lambda$ (middle panel), and $T_c$ (bottom panel) of the clathrate $UH_{10}$ structure at different pressures.

stretching. The high frequency and direct bond vibration contribute to the high EPC parameter $\lambda$, and thus favors high-$T_c$ in these systems. Figure 4b shows the phonon dispersions of clathrate $UH_{10}$ at 300 GPa. The phonon dispersions of clathrate $UH_6$, $UH_9$, and $UH_{10}$ at 200 and 300 GPa are summarized in the Supporting Information (Figures S1–S3). All of the phonon dispersions in the whole first Brillouin zone (BZ) have positive frequencies, indicating their lattice dynamical stabilities.

The electronic DOS at the Fermi level is notably large ($\sim$12 states/cell), which may lead to superconductivity. However, the electronic DOS at the Fermi level is mainly contributed by U-f electrons, and the U atom is enormously heavy, thus its relatively low vibration may destroy the emergence of superconductivity. To study the superconducting properties of these clathrate structures more precisely, we calculated the electronic DOS projected on H atoms, electron–phonon coupling (EPC), and based on them calculated the super-conducting transition temperature using the Dynes-corrected MacMillan's equation.[33]

Figure 4c shows the electronic DOS projected on H atoms, the EPC parameter $\lambda$, and superconducting transition temperature $T_c$. Following the Dynes-corrected MacMillan's equation, $T_c$ is given by

$$T_c = \frac{\omega_{\log}}{1.2} \exp\left(-\frac{1.04(1+\lambda)}{\lambda - \mu^*(1+0.62\lambda)}\right)$$

where $\mu^*$ represents the Coulomb pseudopotential parameter, which was chosen as $\mu^* = 0.1$ and 0.13. Our calculation results show that the DOS projected on H atoms, EPC parameter $\lambda$, and transition temperature $T_c$, all increase with increasing pressure. The detailed values in Figure 4c are listed in Table S1 of the Supporting Information. The EPC parameters $\lambda$ are 0.714, 0.722, and 1.124 at 200, 300, and 400 GPa, respectively. The resulting $T_c$ values are 40.2 (31.1), 74.9 (58.3), and 81.1 (71.2) K using $\mu^* = 0.1$ (0.13) for $UH_{10}$ at 200, 300, and 400 GPa, respectively, which approach the liquid nitrogen temperature 77 K.

The superconductivities of other $f$-electron clathrate structures have been investigated recently, and the predicted $T_c$ for $LaH_9$, $CeH_9$, $CeH_{10}$, and $PrH_9$ is lower than 56 K.[17] Our study on clathrate $UH_{10}$ enhanced the upper limit of the $T_c$ of $f$-electron clathrate structures.

## 3. CONCLUSIONS

In conclusion, we have used first-principles structure searching method to obtain the pressure-induced clathrate uranium hydrides $UH_6$, $UH_9$, and $UH_{10}$, which contain $H_{24}$, $H_{29}$, and $H_{32}$ cages. The U–H bonding in these clathrate structures is ionic, while covalent H–H interactions are evident between the nearest-neighbor H atoms. The clathrate structures exhibit potential high-$T_c$ superconductivity (up to 81.1 K) that originates from relatively strong electron–phonon coupling.

## 4. METHODS AND COMPUTATIONAL DETAILS

To investigate the properties of uranium hydride $UH_x$, a variable-composition structure search has been executed with stoichiometries ranging from $x = 0.5$ to 18.[28] Based on previous results and the clathrate structures of rare earth hydrides,[17] we performed a further precise structure search at high pressures (50–400 GPa) via CALYPSO,[34] which is based on the swarm intelligence method.[35,36] Initial structures were generated randomly and then up to 30 generations were calculated, with each generation containing 40 structures. Then, ab initio density functional theory (DFT)[29] calculations were performed so the structures were optimized to local minimum via the VASP (Vienna Ab initio Simulation Package) code.[37,38] The PAW (projector-augmented wave) method[39] was chosen to describe the electron–ion interaction, and generalized gradient approximation[40] through Perdew–Burke–Ernzerhof functional was adopted to deal with the exchange–correlation potential. Energy cutoff and k-point separation were set as 550 eV and 0.2 Å$^{-1}$, respectively. The energetic convergence threshold was $10^{-6}$ eV and $10^{-2}$ eV/Å for force. Then, the structures of the lowest formation enthalpies could be obtained. Phonon dispersion and electron–phonon coupling (EPC) calculations were performed with density functional perturbation theory. The superconductivity calculations were performed using the Quantum-ESPRESSO package.[41,42] The $q$ and $k$ mesh were chosen as $3 \times 3 \times 3$ and $18 \times 18 \times 18$ for the uranium hydride structure in the first Brillouin zone (BZ) in the EPC calculations.

## ■ ASSOCIATED CONTENT

### ⓈI Supporting Information

The Supporting Information is available free of charge at https://pubs.acs.org/doi/10.1021/acsomega.0c05794.

Snapshots showing band structures, DOS, and phonon spectrum of $UH_6$, $UH_9$, and $UH_{10}$ clathrate structures under 200 and 300 GPa, respectively; DOS of H at the Fermi level ($N_{Ef}$) per Å$^3$, the EPC parameter $\lambda$, and $T_c$ of clathrate $UH_{10}$ structures under different pressures (PDF)

## ■ AUTHOR INFORMATION

### Corresponding Authors

**Jian Liu** − *State Key Laboratory of Heavy Oil, China University of Petroleum-Beijing, Beijing 102249, China;* ⓞ orcid.org/0000-0003-3392-9812; Email: liujian@cup.edu.cn

**Ping Zhang** − *Institute of Applied Physics and Computational Mathematics, Beijing 100088, China; HEDPS, Center for Applied Physics and Technology, Peking University, Beijing 100871, China; Beijing Computational Science Research Center, Beijing 100193, China;* Email: zhang_ping@iapcm.ac.cn

### Authors

**Xiao-hui Wang** − *College of Science, China University of Petroleum-Beijing, Beijing 102249, China;* ⓞ orcid.org/0000-0002-3353-3140

**Fa-wei Zheng** − *Institute of Applied Physics and Computational Mathematics, Beijing 100088, China*

**Zhuo-wei Gu** − *Institute of Fluid Physics, China Academy of Engineering Physics, Mianyang 621900, China*

**Fu-li Tan** − *Institute of Fluid Physics, China Academy of Engineering Physics, Mianyang 621900, China*

**Jian-heng Zhao** − *Institute of Fluid Physics, China Academy of Engineering Physics, Mianyang 621900, China*

**Cang-li Liu** − *Institute of Fluid Physics, China Academy of Engineering Physics, Mianyang 621900, China*

**Cheng-wei Sun** − *Institute of Fluid Physics, China Academy of Engineering Physics, Mianyang 621900, China*

Complete contact information is available at:
https://pubs.acs.org/10.1021/acsomega.0c05794

### Notes

The authors declare no competing financial interest.

## ■ REFERENCES

(1) Wigner, E.; Huntington, H. B. On the Possibility of a Metallic Modification of Hydrogen. *J. Chem. Phys.* **1935**, *3*, 764–770.

(2) Ashcroft, N. W. Metallic hydrogen: A high-temperature superconductor? *Phys. Rev. Lett.* **1968**, *21*, 1748.

(3) Loubeyre, P.; Occelli, F.; LeToullec, R. Optical studies of solid hydrogen to 320 GPa and evidence for black hydrogen. *Nature* **2002**, *416*, 613–617.

(4) Dalladay-Simpson, P.; Howie, R. T.; Gregoryanz, E. Evidence for a new phase of dense hydrogen above 325 gigapascals. *Nature* **2016**, *529*, 63–67.

(5) Zha, C. S.; Liu, Z.; Hemley, R. J. Synchrotron infrared measurements of dense hydrogen to 360 GPa. *Phys. Rev. Lett.* **2012**, *108*, No. 146402.

(6) Dias, R. P.; Silvera, I. F. Observation of the Wigner-Huntington transition to metallic hydrogen. *Science* **2017**, *355*, 715–718.

(7) Ashcroft, N. W. Hydrogen Dominant Metallic Alloys: High Temperature Superconductors? *Phys. Rev. Lett.* **2004**, *92*, No. 187002.

(8) Gao, G.; Oganov, A. R.; Bergara, A.; Martinez-Canales, M.; Cui, T.; Iitaka, T.; Ma, Y.; Zou, G. Superconducting high pressure phase of germane. *Phys. Rev. Lett.* **2008**, *101*, No. 107002.

(9) Li, Y.; Gao, G.; Xie, Y.; Ma, Y.; Cui, T.; Zou, G. Superconductivity at ~100 K in dense SiH4 (H2) 2 predicted by first principles. *Proc. Natl. Acad. Sci. U.S.A.* **2010**, *107*, 15708–15711.

(10) Wang, H.; John, S. T.; Tanaka, K.; Iitaka, T.; Ma, Y. Superconductive sodalite-like clathrate calcium hydride at high pressures. *Proc. Natl. Acad. Sci. U.S.A.* **2012**, *109*, 6463–6466.

(11) Drozdov, A. P.; Eremets, M. I.; Troyan, I. A.; Ksenofontov, V.; Shylin, S. I. Conventional superconductivity at 203 kelvin at high pressures in the sulfur hydride system. *Nature* **2015**, *525*, 73–76.

(12) Einaga, M.; Sakata, M.; Ishikawa, T.; Shimizu, K.; Eremets, M. I.; Drozdov, A. P.; Troyan, I. A.; Hirao, N.; Ohishi, Y. Crystal structure of the superconducting phase of sulfur hydride. *Nat. Phys.* **2016**, *12*, 835–838.

(13) Geballe, Z. M.; Liu, H.; Mishra, A. K.; Ahart, M.; Somayazulu, M.; Meng, Y.; Baldini, M.; Hemley, R. J. Synthesis and Stability of Lanthanum Superhydrides. *Angew. Chem., Int. Ed.* **2018**, *57*, 688–692.

(14) Liu, H.; Naumov, I. I.; Hoffmann, R.; Ashcroft, N. W.; Hemley, R. J. Potential high-Tc superconducting lanthanum and yttrium hydrides at high pressure. *Proc. Natl. Acad. Sci. U.S.A.* **2017**, *114*, 6990.

(15) Huang, X.; Wang, X.; Duan, D.; Sundqvist, B.; Li, X.; Huang, Y.; Yu, H.; Li, F.; Zhou, Q.; Liu, B.; Cui, T. High-temperature superconductivity in sulfur hydride evidenced by alternating-current magnetic susceptibility. *Natl. Sci. Rev.* **2019**, *6*, 713–718.

(16) Somayazulu, M.; Ahart, M.; Mishra, A. K.; Geballe, Z. M.; Baldini, M.; Meng, Y.; Struzhkin, V. V.; Hemley, R. J. Evidence for Superconductivity above 260 K in Lanthanum Superhydride at Megabar Pressures. *Phys. Rev. Lett.* **2019**, *122*, No. 027001.

(17) Peng, F.; Sun, Y.; Pickard, C. J.; Needs, R. J.; Wu, Q.; Ma, Y. Hydrogen clathrate structures in rare earth hydrides at high pressures: Possible route to room-temperature superconductivity. *Phys. Rev. Lett.* **2017**, *119*, No. 107001.

(18) Oganov, A. R.; Pickard, C. J.; Zhu, Q.; Needs, R. J. Structure prediction drives materials discovery. Nature Reviews. *Materials* **2019**, *4*, 331–348.

(19) Li, X.; Huang, X.; Duan, D.; Pickard, C. J.; Zhou, D.; Xie, H.; Zhuang, Q.; Huang, Y.; Zhou, Q.; Liu, B.; Cui, T. Polyhydride CeH9 with an atomic-like hydrogen clathrate structure. *Nat. Commun.* **2019**, *10*, No. 3461.

(20) Sun, Y.; Lv, J.; Xie, Y.; Liu, H.; Ma, Y. Route to a Superconducting Phase above Room Temperature in Electron-Doped Hydride Compounds under High Pressure. *Phys. Rev. Lett.* **2019**, *123*, No. 097001.

(21) Lonie, D. C.; Hooper, J.; Altintas, B.; Zurek, E. Metallization of magnesium polyhydrides under pressure. *Phys. Rev. B* **2013**, *87*, No. 054107.

(22) Fu, Y. H.; Du, X. P.; Zhang, L. J.; Peng, F.; Zhang, M.; Pickard, C. J.; Needs, R. J.; Singh, D. J.; Zheng, W. T.; Ma, Y. M. High-Pressure Phase Stability and Superconductivity of Pnictogen Hydrides and Chemical Trends for Compressed Hydrides. *Chem. Mater.* **2016**, *28*, 1746–1755.

(23) Li, Y.; Hao, J.; Liu, H.; Tse, J. S.; Wang, Y.; Ma, Y. Pressure-stabilized superconductive yttrium hydrides. *Sci. Rep.* **2015**, *5*, No. 9948.

(24) Kvashnin, A. G.; Semenok, D. V.; Kruglov, I. A.; Wrona, I. A.; Oganov, A. R. High-Temperature Superconductivity in a Th−H

System under Pressure Conditions. *ACS Appl. Mater. Interfaces* **2018**, *10*, 43809–43816.

(25) Semenok, D. V.; Kvashnin, A. G.; Kruglov, I. A.; Oganov, A. R. Actinium Hydrides AcH10, AcH12, and AcH16 as High-Temperature Conventional Superconductors. *J. Phys. Chem. Lett.* **2018**, *9*, 1920–1926.

(26) Kruglov, I. A.; Kvashnin, A. G.; Goncharov, A. F.; Oganov, A. R.; Lobanov, S. S.; Holtgrewe, N.; Jiang, S.; Prakapenka, V. B.; Greenberg, E.; Yanilkin, A. V. Uranium polyhydrides at moderate pressures: Prediction, synthesis, and expected superconductivity. *Sci. Adv.* **2018**, *4*, No. eaat9776.

(27) Allred, A. L. Electronegativity values from thermochemical data. *J. Inorg. Nucl. Chem.* **1961**, *17*, 215–221.

(28) Wang, X.; Li, M.; Zheng, F.; Zhang, P. Crystal structure prediction of uranium hydrides at high pressure: A new hydrogen-rich phase. *Phys. Lett. A* **2018**, *382*, 2959–2964.

(29) Becke, A. D.; Edgecombe, K. E. A simple measure of electron localization in atomic and molecular systems. *J. Chem. Phys.* **1990**, *92*, 5397–5403.

(30) McMahon, J. M.; Ceperley, D. M. Ground-State Structures of Atomic Metallic Hydrogen. *Phys. Rev. Lett.* **2011**, *106*, No. 165302.

(31) Bader, R. F. W. *Atoms in Molecules: A Quantum Theory:*; Oxford University Press: Oxford, 1990.

(32) Henkelman, G.; Arnaldsson, A.; Jónsson, H. A fast and robust algorithm for Bader decomposition of charge density. *Comput. Mater. Sci.* **2006**, *36*, 354–360.

(33) Dynes, R. C. McMillan's equation and the Tc of superconductors. *Solid State Communications* **1972**, *10*, 615–618.

(34) Wang, Y.; Lv, J.; Zhu, L.; Ma, Y. CALYPSO: A method for crystal structure prediction. *Comput. Phys. Commun.* **2012**, *183*, 2063–2070.

(35) Wang, Y.; Lv, J.; Zhu, L.; Ma, Y. Crystal structure prediction via particle-swarm optimization. *Phys. Rev. B* **2010**, *82*, No. 094116.

(36) Lu, C.; Miao, M.; Ma, Y. Structural evolution of carbon dioxide under high pressure. *J. Am. Chem. Soc.* **2013**, *135*, 14167–14171.

(37) Kresse, G.; Furthmüller, J. Efficiency of ab-initio total energy calculations for metals and semiconductors using a plane-wave basis set. *Comput. Mater. Sci.* **1996**, *6*, 15–50.

(38) Kresse, G.; Furthmüller, J. Efficient iterative schemes for ab initio total-energy calculations using a plane-wave basis set. *Phys. Rev. B* **1996**, *54*, 11169.

(39) Blöchl, P. E. Projector augmented-wave method. *Phys. Rev. B* **1994**, *50*, 17953.

(40) Perdew, J. P.; Burke, K.; Ernzerhof, M. Generalized gradient approximation made simple. *Phys. Rev. Lett.* **1996**, *77*, 3865.

(41) Giannozzi, P.; Baroni, S.; Bonini, N.; Calandra, M.; Car, R.; Cavazzoni, C.; Ceresoli, D.; Chiarotti, G. L.; Cococcioni, M.; Dabo, I.; et al. QUANTUM ESPRESSO: a modular and open-source software project for quantum simulations of materials. *J. Phys.: Condens. Matter* **2009**, *21*, No. 395502.

(42) Giannozzi, P.; Andreussi, O.; Brumme, T.; Bunau, O.; Nardelli, M. B.; Calandra, M.; Car, R.; Cavazzoni, C.; Ceresoli, D.; Cococcioni, M.; et al. Advanced capabilities for materials modelling with Quantum ESPRESSO. *J. Phys.: Condens. Matter* **2017**, *29*, No. 465901.